A theoretical study of the quantum states of hydrogen in niobium

1991 J. Phys.: Condens. Matter 3 9429

(http://iopscience.iop.org/0953-8984/3/47/015)

J. Phys.: Condens. Matter 3 (1991) 9429–9445. Printed in the UK

A theoretical study of the quantum states of hydrogen in niobium

F Christodoulos and M J Gillan
Physics Department, University of Keele, Keele, Staffordshire ST5 5BG, UK

Received 15 July 1991

Abstract. We present calculations of the energies and wavefunctions for the vibrational ground state and over 40 excited states of a hydrogen impurity in niobium. Predictions are also given for the transition intensities measured by neutron scattering. The calculations are based on an interaction model for the niobium–hydrogen system developed previously. The aims of the work are to investigate the nature of the quantum states and to show how comparisons of the energies and transition intensities with experiment can be used to test the interaction model. It is shown that for excitation energies above ~ 0.2 eV, many of the states differ greatly from the harmonic oscillator states often assumed in previous analyses. Agreement of the excitation energies and intensities with experimental data is fairly good, though problems of assignment for higher experimental transitions hamper the comparison. It is suggested further that calculations of the present kind will help resolve these problems.

1. Introduction

In a series of recent papers (Gillan 1986, 1987, 1988, 1990, 1991, Christodoulos and Gillan 1991) we have sought to interpret the observed properties of hydrogen in transition metals, for example the diffusion coefficient and the results of diffraction measurements, in terms of models for the interactions between the atoms. The present paper is concerned with the interpretation of neutron inelastic scattering experiments, which should be one of the most fruitful sources of information about the metal–hydrogen interaction (Springer 1978, Eckert *et al* 1983, Ikeda and Watanabe 1987, Ikeda *et al* 1990). In these experiments, the scattered neutron probes the dynamics of dissolved hydrogen by inducing transitions, normally between the vibrational ground state and the excited quantum states. The transitions are observed as peaks in the energy-dependent scattering cross-section. The energies of these peaks give the energy differences between the quantum states, and their wavevector-dependent intensities give information about the wavefunctions of the states (Ikeda *et al* 1990). Both the energies and the wavefunctions are governed by the potential in which the hydrogen moves. In principle, therefore, the inelastic measurements can tell us much about this potential. However, a full interpretation of such measurements demands a good understanding of the nature of the potential and of the excited states. Our purpose in the present paper is to help this understanding by presenting the results of calculations of the energy and wavefunctions of an extensive series of quantum states for hydrogen in niobium. The calculations are based on a simple interaction model for

0953-8984/91/479429+17$03.50

this system developed in our earlier work. The comparisons with experiment that we shall present both for the transition energies and the scattering intensities will confirm the usefulness of the model, but will also point the way to more stringent tests.

In early neutron work on H in Nb and related BCC systems (for a review, see Springer 1978), the beam intensity was enough only to reveal the two prominent peaks of lowest energy in the inelastic cross-section. Since hydrogen occupies the tetrahedral interstitial site, which has tetragonal D_{2d} symmetry (see figure 1), there are two independent vibrational frequencies; transitions from the ground state to the first excited oscillator states for motion along and perpendicular to the tetragonal axis give rise to the two prominent peaks. At that time, all that could be said was that the potential acting on the hydrogen was like a three-dimensional oscillator with two independent frequencies. Improvements in beam intensity led to the observation of transitions to higher states, as well as to experiments on other isotopes, which showed that deviations from harmonic behaviour were readily detectable (Eckert *et al* 1983). A common way to analyse the results has been to add to the harmonic potential anharmonic components consistent with the D_{2d} symmetry, which are treated by perturbation theory; the coefficients of the anharmonic components are then used as fitting parameters. The method was used by Ikeda and Watanabe (1987) to analyse their recent experiments, which are remarkable in revealing no less than 10 transitions up to an excitation energy of 0.5 eV.

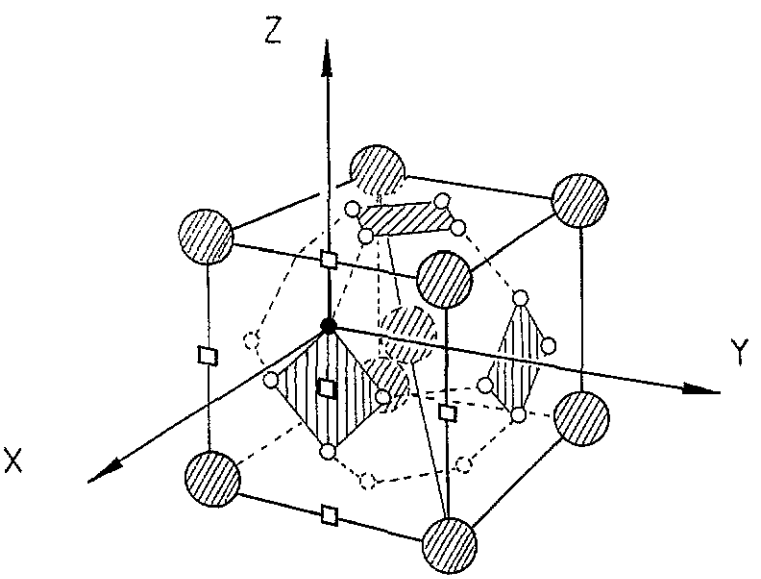

Figure 1. The tetrahedral interstitial sites occupied by hydrogen in niobium. Large and small circles represent niobium atoms and tetrahedral sites respectively. For the tetrahedral site marked by a filled circle, the z axis is the tetragonal axis, and the x and y axes are equivalent directions perpendicular to this axis. Selected octahedral positions are marked by a square.

We shall show here that for quite moderate excitation energies (above ~ 0.2 eV), the potential deviates very strongly from the harmonic form, and that the anharmonic perturbation approach is likely to be misleading. Our calculations are not based on this approach, but on the ideas pioneered by Sugimoto and Fukai (1980, 1981, 1982)

(see also Fukai and Sugimoto 1985) and used by a number of other authors (e.g. Puska and Nieminen 1984, Klamt and Teichler 1986). We start from an explicit model for the total energy of the system as a function of the positions of the hydrogen and metal atoms. The ground state is then determined as the lowest-energy solution of the Schrödinger equation for hydrogen, with the metal atoms relaxed to equilibrium. The excited states are found by solving the Schrödinger equation for hydrogen with the metal atoms held fixed in the relaxed positions found for the ground state: it is assumed that the metal atoms are immobile in the excitation process. The Schrödinger equation is not treated by perturbation theory: it is solved numerically on a grid. There is a very important reason for basing the calculations on a model interaction function for the total energy of the system, namely that one can then use exactly the same interaction model as is used in treating a range of other properties: diffusion coefficient, diffraction intensities, diffuse-scattering intensities, tunnelling frequencies, etc. In addition, one explicitly recognizes that the potential acting on the hydrogen is strongly conditioned by the process of self-trapping, i.e. the relaxation of the metal lattice in response to the presence of hydrogen at an interstitial site.

Although we build on the work of Sugimoto and Fukai, we go considerably further than them. They were hampered by the technical problems of solving the Schrödinger equation for a complicated three-dimensional system, and succeeded in treating only a few of the lowest states. This did not matter at the time, since only these few states were observable then, but the rapid progress in experimental technique means that the much more extensive survey presented here is now needed. The more powerful numerical techniques we use allow us to treat more than 40 states, with excitation energies going up to over 0.5 eV.

The paper is organized as follows. Section 2 describes the techniques we have used to solve the Schrödinger equation, perform the relaxation to ground-state equilibrium and calculate the inelastic scattering intensities. In section 3, we summarize the tests we have applied to ensure that the solutions of the Schrödinger equation are fully converged with respect to the grid spacing and the size of the region in which the calculations are performed. The main results are presented in section 4, where we display the calculated potential acting on hydrogen, tabulate the energies of the states, classified according to their symmetry, and compare with the experimental energies. We also show plots of the wavefunctions for the ground state and some representative states of higher energies, and show how they can be qualitatively understood as linear combinations of oscillator states associated with the central site and neighbouring sites. In section 5, we present results for the scattering intensities of the full set of states we have treated, and compare with the presently available data. The paper concludes with a brief discussion of the results.

2. Theoretical basis of the calculations

2.1. The quantities to be calculated

Before describing the technical details of the calculations, we first outline what we are attempting to calculate. Inelastic neutron scattering probes transitions between initial and final quantum states of the hydrogen. We study here only transitions from the vibrational ground state. This is normally the case of interest, since the temperatures at which the experiments are performed are usually low enough for the occupation probability of higher states to be small. In treating the ground state, we ignore the

vibrations of the metal atoms. However, a crucial effect which must be included is the relaxation of the metal atoms from their regular positions due to the repulsive metal–hydrogen interaction. This relaxation produces a lowering of the potential $w(\boldsymbol{r})$ acting on the hydrogen at the occupied site, which is responsible for self-trapping. Our first task is therefore to calculate the lattice displacements, the potential $w(\boldsymbol{r})$ and the hydrogen wavefunction for the relaxed ground state.

Our next task is to calculate the energy eigenvalues and eigenfunctions for the excited states. In doing this, we take the potential acting on the hydrogen to be the $w(\boldsymbol{r})$ appropriate to the relaxed ground state. We are thus treating the metal atoms as classical particles which remain immobile during the transition. This is an approximation: the thermal and quantum fluctuations of the metal lattice produce a broadening of the transition lines, which we ignore. The approximation is exactly equivalent to the well-known Franck–Condon principle in the theory of optical transitions in crystals. It is a standard result of that theory that the Franck–Condon principle correctly gives the mean transition energy of each line, provided the coupling with the lattice is linear (see e.g. Stoneham 1975, section 10.8). The work reported in the present paper does not depend on the approximation of linear coupling, but the approximation should nonetheless be an excellent one. This means that our treatment of the metal lattice as immobile should be fully justified.

Our final task is to use the calculated eigenfunctions to obtain the wavevector-dependent neutron scattering intensities for each transition.

2.2. The interaction model

The calculations are based on our previous model (Gillan 1987, Christodoulos and Gillan 1991) for the energy $U(\{\boldsymbol{R}_i\},\boldsymbol{r})$ of the niobium–hydrogen system as a function of the positions $\boldsymbol{R}_i$ of all the metal atoms and the position $\boldsymbol{r}$ of the single hydrogen impurity. As usual, the Born–Oppenheimer approximation for the electrons is assumed—we are not concerned here with the effects of electronic non-adiabaticity which are observed at low temperatures (Kondo 1985)—so that U is the total energy of the electronic ground state as a function of the positions $\boldsymbol{R}_i$ and $\boldsymbol{r}$ treated as classical parameters. This energy is represented as the sum of the energy $U_{\mathrm{M}}(\{\boldsymbol{R}_i\})$ of the pure metal system, and the energy $U_{\mathrm{MH}}(\{\boldsymbol{R}_i\},\boldsymbol{r})$ of interaction of the hydrogen with the metal system:

$$U = U_{\mathrm{M}} + U_{\mathrm{MH}}\,. \tag{1}$$

For U_{M}, we take the Finnis–Sinclair model, with the parameters given previously (Gillan 1987). Since the response of the metal system to the forces exerted by hydrogen is particularly important in the present work, we need to know that the vibrational frequencies of the pure metal are approximately correct. We have verified that the phonon dispersion relations of niobium calculated from our model for U_{M} agree quite satisfactorily with experiment.

The metal–hydrogen energy is represented as a sum of pair potentials:

$$U_{\mathrm{MH}}(\{\boldsymbol{R}_i\},\boldsymbol{r}) = \sum_i V_{\mathrm{MH}}(|\boldsymbol{r}-\boldsymbol{R}_i|) \tag{2}$$

where

$$V_{\mathrm{MH}}(r) = B\exp(-r/\sigma) \tag{3}$$

with the parameters $B = 25\,716$ eV and $\sigma = 0.162$ Å given previously. It should be noted that with a pair potential of this form one cannot reproduce the experimental values for the components of the elastic dipole tensor $\boldsymbol{P}$ (Sugimoto and Fukai 1980). It has been shown by Sugimoto and Fukai (1980) that these can be reproduced if one is prepared to include in $V_{MH}(r)$ a long-range contribution, which they represent by a second exponential. The physical origin of such a contribution has never been made clear, and we do not feel that it is acceptable to proceed in this way. We prefer instead to tolerate the discrepancy with the measured components of $\boldsymbol{P}$. The properties of the localized quantum states will in any case be determined mainly by short-range interactions.

2.3. The numerical solution of the Schrödinger equation

For a given set of metal–atom positions, we have to solve the Schrödinger equation for hydrogen acted on by the potential $w(\boldsymbol{r})$ given by

$$w(\boldsymbol{r}) = \sum_i V_{MH}(|\boldsymbol{r} - \boldsymbol{R}_i|)\,. \tag{4}$$

We calculate the energy eigenvalues and eigenfunctions by the usual finite-difference approximation. The eigenfunctions $\psi(\boldsymbol{r})$ are represented by their values on a cubic mesh having mesh length δr in a cubic box of length $L = N\delta r$, with the condition that ψ vanishes on the boundaries of the box. Let $\psi(i,j,k)$ be the value of ψ on the mesh-point whose Cartesian coordinates are $(i,j,k)\delta r$. Then, using the simplest finite-difference approximation to the Laplacian $\nabla^2\psi$ the Schrödinger equation is represented as the matrix eigenvalue equation:

$$\begin{aligned} -(\hbar^2/2m\delta r^2)[&\psi(i+1,j,k) + \psi(i-1,j,k) + \psi(i,j+1,k) + \psi(i,j-1,k) \\ &+ \psi(i,j,k+1) + \psi(i,j,k-1) - 6\psi(i,j,k)] + w(i,j,k)\psi(i,j,k) \\ &= E\psi(i,j,k)\,. \end{aligned} \tag{5}$$

Instead of the Kimball and Shortley (1934) technique used by Sugimoto and Fukai (1980), which we have found to be extremely inefficient, we have used the standard matrix diagonalization routines provided in the NAG library. One should be aware that the dimension of the matrix is very large. Since the number of mesh-points N in each direction needs to be at least of order 30, the dimension of the matrix $M = N^3$ is typically several times 10^4 or greater. It is therefore essential to exploit the sparseness of the matrix, and to use a method which calculates only a specified number of the lowest eigenvalues. Provided this is done, the computation time scales as M, and the problem becomes tractable.

The computation time is further greatly reduced by exploiting the symmetry of the system. The cubic solution box is centred at the tetrahedral site, which has D_{2d} symmetry. Here and throughout the following discussion, we use the Cartesian axes shown in figure 1. The tetragonal axis at the occupied site, namely the cubic axis passing through this site and the two nearest octahedral sites, is the z axis; the x and y axes are the other two cubic axes. The D_{2d} point group is of order 8. It has four one-dimensional irreducible representations A_1, A_2, B_1, B_2 and a two-dimensional representation E; these transform like the functions 1, xyz, xy, z (or equivalently x^2-y^2) and (x,y) respectively. By taking appropriate linear combinations

of the $\psi(i,j,k)$, the Hamiltonian matrix is block-diagonalized with respect to these representations, and the remaining diagonalization can then be performed separately for each representation. The symmetry-based techniques for doing this are standard, and are described by e.g. Atkins (1983). By these means, it is straightforward to perform calculations with the number of mesh-points N equal to 50 or greater.

In the calculations to be reported in sections 4 and 5, the box length L has been taken equal to the lattice parameter a_0 (the side of the BCC cube). We have made extensive tests of the convergence of the results with respect to both L and the mesh length δr, which are described in section 3.

2.4. Lattice relaxation

We have determined the equilibrium displacements of the metal atoms in the ground state by an iterative method similar to that used by Sugimoto and Fukai (1980). For a given set of metal-atom positions $\boldsymbol{R}_i$, we calculate the potential $w(\boldsymbol{r})$ on the grid from equation (4) and solve the Schrödinger equation to determine the ground state eigenfunction ψ_0. The force $\boldsymbol{F}_i^{\mathrm{H}}$ exerted by the hydrogen on metal atom i is then calculated as:

$$\boldsymbol{F}_i^{\mathrm{H}} = -\nabla_{\boldsymbol{R}_i} \int \mathrm{d}\boldsymbol{r}\ \psi_0(\boldsymbol{r})^2 V_{\mathrm{MH}}(|\boldsymbol{r}-\boldsymbol{R}_i|)\,. \tag{6}$$

By adding the force $-\nabla_{\boldsymbol{R}_i} U_{\mathrm{M}}$, we obtain the total force $\boldsymbol{F}_i^{\mathrm{tot}}$ on metal atom i. Each metal atom is now moved from its current position by an amount $\delta\boldsymbol{R}_i = k\boldsymbol{F}_i^{\mathrm{tot}}$, where k is a constant which is the same for all metal atoms, and is held fixed throughout the iterative process. The potential $w(\boldsymbol{r})$ is now recalculated for the new $\boldsymbol{R}_i$, and the process is repeated until the ground-state energy has converged to within a specified accuracy. For a suitably chosen value of k the convergence is extremely rapid, and equilibrium is attained within typically 5 iterations or less.

2.5. The scattering intensities

For a given orientation of the crystal, and a given wavevector transfer $\boldsymbol{Q}$, the inelastic scattering intensity $I_i(\boldsymbol{Q})$ for transitions from the ground-state to a specified excited state i is (apart from trivial constants) given by:

$$I_i(\boldsymbol{Q}) = |M_i(\boldsymbol{Q})|^2 \tag{7}$$

where $M_i(\boldsymbol{Q})$ is a matrix element given by:

$$M_i(\boldsymbol{Q}) = \int \mathrm{d}\boldsymbol{r}\ \psi_i(\boldsymbol{r})^* \mathrm{e}^{\mathrm{i}\boldsymbol{Q}\cdot\boldsymbol{r}} \psi_0(\boldsymbol{r})\,. \tag{8}$$

We approximate this integral by a summation on the mesh. It should be noted that since we are dealing here with a Fourier transformation, summation on a mesh can in principle give rise to aliasing errors. We have checked that with the mesh lengths used here, such errors are negligible for the Q values of interest.

One final step is needed. For most experiments performed to date, powder specimens rather than single crystals are used. This means that the measured intensity is the spherical average of $I_i(\boldsymbol{Q})$, which we denote by $\langle I_i(\boldsymbol{Q})\rangle$. For each magnitude $|\boldsymbol{Q}|$,

we calculate $I_i(\boldsymbol{Q})$ for a set of orientations of $\boldsymbol{Q}$, specified by polar angles θ and ϕ. The two-dimensional integral needed to obtain the angular average:

$$\langle I_i(\boldsymbol{Q})\rangle = \frac{1}{4\pi}\int_0^{2\pi} \mathrm{d}\phi \int_0^{\pi} \mathrm{d}\theta \sin\theta I_i(\boldsymbol{Q}) \tag{9}$$

is then approximated numerically. Again, systematic checks have been performed to ensure that integration errors are insignificant.

3. Convergence tests

Two approximations are made in solving the Schrödinger equation: the Laplacian is replaced by a finite difference, and the solution is performed in a finite box. In order to check that the finite-difference error is negligible, we investigated the variation of all our calculated eigenvalues for a range of mesh lengths δr. We illustrate the results of these tests in figure 2, which shows the variation of the energies of the ground state and two representative excited states for a box length L equal to the lattice parameter a_0. The positions of the metal atoms, and hence the potential $w(\boldsymbol{r})$, are the same for all these calculations; we use the relaxed metal–atom positions obtained for $\delta r = 0.092$ Å and $L = a_0$. We have checked that this value of δr is more than adequate for the calculation of these relaxed positions. It is clear from this figure that for $\delta r = 0.06$ Å, which is easily attainable, the residual error in the eigenvalues is no more than a few meV, which is quite acceptable. Even this slight error could be eliminated by extrapolation, if necessary.

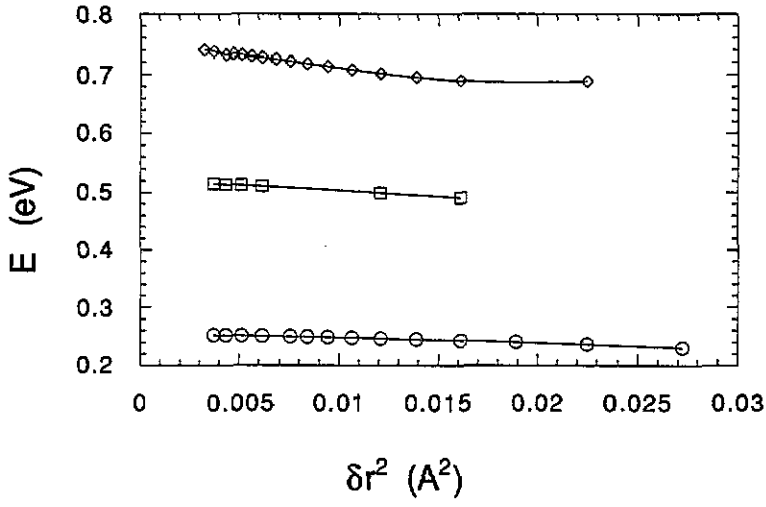

Figure 2. Variation of calculated energy eigenvalues with mesh length δr. Energies are shown for the ground state (circles), the state E(3) (squares), and the state $A_2(2)$ (diamonds) (see text in section 3 for notation). In all cases the Schrödinger equation is solved with the boundary condition that the wavefunction vanishes on the surface of a box whose length is equal to the lattice parameter a_0.

We have tested the dependence on L by repeating some of the calculations for values of L up to 1.86 a_0, with δr held fixed. We find that for all the states of interest here, the variation of the eigenvalues is considerably less than 1 meV, and is therefore utterly negligible.

4. The quantum states

4.1. The ground state

The methods outlined above have been applied first to study the relaxed ground state. For this purpose, the solution of the Schrödinger equation was obtained with the mesh length $\delta r = 0.092$ Å.

The repulsive forces exerted by the hydrogen impurity on the metal atoms cause the latter to relax outwards. When equilibrium is achieved, with hydrogen in its ground state, the displacements of the four nearest neighbours have components in the $x-y$ plane and in the z direction (see figure 1) equal to 0.081 and 0.043 Å. The magnitude of the displacement is therefore 0.092 Å, which agrees satisfactorily with the value of 0.10 Å deduced from diffuse scattering measurements (Peisl 1982). We define the relaxation energy ΔE_{tot} to be the difference of the total energies of the system with the hydrogen in its ground state when (1) all metal atoms are fixed at their regular positions, and (2) all metal atoms are relaxed to equilibrium. The value we find for ΔE_{tot} is 0.35 eV. This is somewhat less than the value of 0.48 eV found by Sugimoto and Fukai (1980).

The potential field $w(\mathbf{r})$ acting on the hydrogen is, of course, strongly affected by the relaxation of the lattice. Without relaxation, the potential has the full periodicity of the lattice. The relaxation of the neighbours causes a deepening of the potential well at the occupied site, which is responsible for the self-trapping. These effects can be seen in figure 3, which shows contour plots of the unrelaxed and relaxed potentials on the y–z plane passing through the occupied site (see figure 1). In the relaxed system, the minimum at the central site is about 0.19 eV below the minima at the

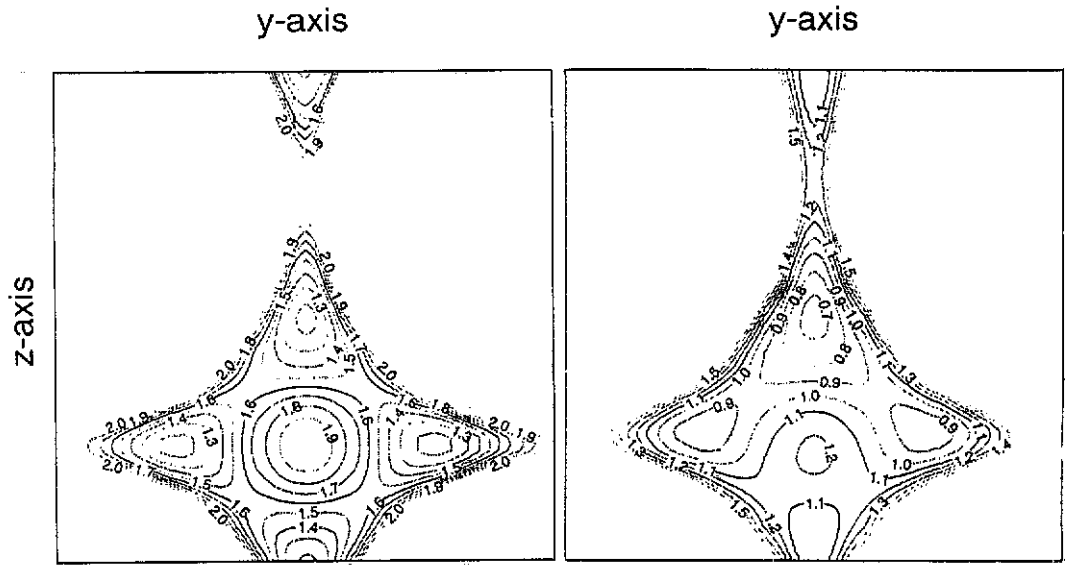

Figure 3. Contour plots of the potential $w(\mathbf{r})$ acting on hydrogen in the unrelaxed ground state (left); the fully relaxed ground state (right). The plots show $w(\mathbf{r})$ on the y–z plane passing through the central tetrahedral site (see figure 1), the edges of the plot in each direction being equal to the lattice parameter a_0. The axes are oriented as in figure 1. Energies marked on contours are in eV.

four neighbouring tetrahedral sites, and about 0.50 eV below the minimum in the unrelaxed system. The central minimum is separated from the neighbouring minima by saddle points, which, in the relaxed system, lie 0.27 eV above the central minimum. The strong deviations of the potential from quadratic behaviour at rather modest energies above the minimum are apparent.

The ground-state energy eigenvalues (i.e. the sum of the hydrogen–metal interaction and the kinetic energy of the hydrogen) are 1.48 and 0.91 eV in the unrelaxed and relaxed systems. The relaxational lowering of the eigenvalue ΔE_{eig} is thus 0.57 eV. This eigenvalue lowering also determines the threshold for localization of excited states: states whose eigenvalues are less than ΔE_{eig} above the ground state are localized, while those having eigenvalues greater than this are delocalized. We note that the ground-state eigenvalue in the relaxed system is 0.25 eV above the bottom of the potential well.

The ground-state eigenfunction in the relaxed system is shown in figure 4. Its elongation along the tetragonal axis is expected, because the curvature of the potential well is smaller in this direction (see figure 3). Substantial deviations from the inversion symmetry that would exist for a harmonic oscillator are evident.

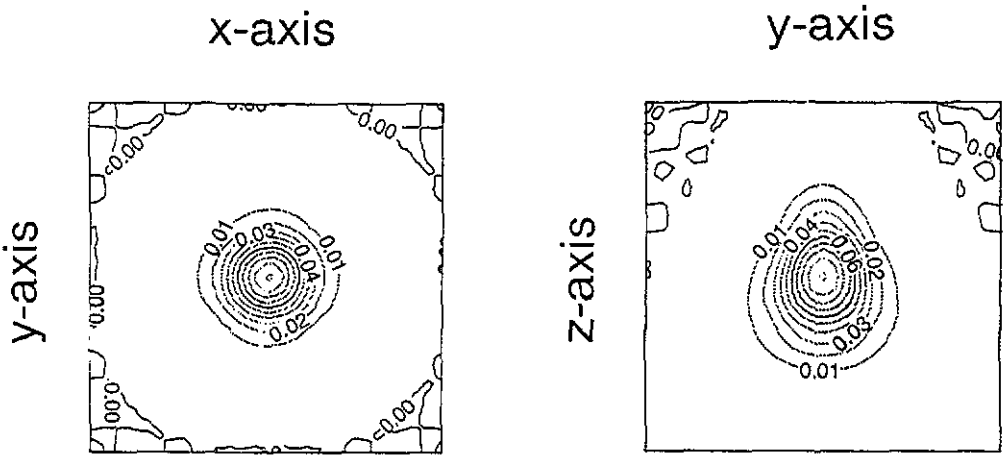

Figure 4. The ground-state wavefunction in the relaxed system shown as contour plots on the x–y plane (left); the y–z plane (right) (see figure 1). The edges of the plots are $\frac{1}{2}a_0$ in each direction.

4.2. The excited states

Using the potential associated with the relaxed ground state, we have solved the Schrödinger equation to determine all the eigenstates up to an energy 0.5 eV above the ground state. The mesh length used in the calculations was 0.062 Å. The energies of the states are listed in table 1. The left-hand column of the table provides for each state an identifying label of the form $R(n)$, which means the nth state in order of increasing energy belonging to irreducible representation R. We cannot, of course, describe all these states in detail here, and there would be little point in doing so. We shall describe the easily observable lowest states, and then illustrate some important features of the higher states by referring to particular examples.

Table 1. The calculated eigenstates for hydrogen in niobium. States are identified in column 1 by the irreducible representation and a sequential index, and in column 2 by a representation in terms of oscillator states on the central and neighbouring tetrahedral sites (see text). The quantities E and ΔE (columns 3 and 4) are respectively the energy relative to the minimum of the potential and the energy relative to the ground state. Experimental values of ΔE (column 5) are marked with an asterisk where we regard the assignment as uncertain. Columns 6–8 give the transition intensity for $Q = 8$ Å^{-1}, the maximum intensity, and the wavevector Q_{max} at which this maximum is attained.

State	Oscillator State	E (calc) (meV)	ΔE (calc) (meV)	ΔE (exp) (meV)	$I(Q = 8$ Å$^{-1})$	$I(Q_{max})$	Q_{max} (Å^{-1})
$A_1(1)$	(000)	253	0	—	—	—	—
$A_1(2)$	(002)/[000]	448	195	—	0.0117	0.0148	11
$A_1(3)$	(002)/[000]	458	205	220	0.0366	0.0486	11
$A_1(4)$	(200)+(020)/[001]	541	288	—	0.0047	0.0117	14
$A_1(5)$	(200)+(020)/[001]	580	327	323*	0.0132	0.0279	14
$A_1(6)$	(004)/[001]	614	361	345*	0.0054	0.0243	15
$A_1(7)$	(004)/[100]	632	379	—	0.0007	0.0091	16
$A_1(8)$	(004)/[100]	665	412	—	0.0044	0.0197	16
$A_1(9)$	{000}	677	424	—	0.0002	0.0015	17
$A_1(10)$	(002)	693	440	—	0.0017	0.0148	17
$A_1(11)$		740	487	—	0.0018	0.0122	18
$A_1(12)$		756	503	—	2.9×10^{-5}	0.0098	19
$A_2(1)$	[010]	685	432	—	2.3×10^{-6}	7.9×10^{-6}	15
$A_2(2)$	(111)	738	485	—	0.002	0.0096	15
$A_2(3)$	[011]	794	541	—	3.7×10^{-5}	4.8×10^{-4}	18
$B_1(1)$	(110)	639	386	372*	0.0129	0.0302	14
$B_1(2)$	[010]	685	432	—	2.1×10^{-6}	8.4×10^{-6}	15
$B_1(3)$		789	536	—	1.3×10^{-4}	0.0017	17
$B_2(1)$	(001)	361	108	115	0.1404	0.1404	8
$B_2(2)$	[000]	450	197	—	3.6×10^{-4}	5×10^{-4}	11
$B_2(3)$	(003)/[001]	520	267	271	0.0129	0.0295	13
$B_2(4)$	(003)/[001]	569	316	—	0.004	0.0187	15
$B_2(5)$	(200)−(020)	586	333	323*	0.0096	0.0196	13
$B_2(6)$	[100]	620	367	—	0.0021	0.0077	15
$B_2(7)$	[002]	657	404	—	0.0019	0.0124	16
$B_2(8)$	{000}	665	412	—	0.0014	0.0078	17
$B_2(9)$	{000}	689	436	—	0.0011	0.0073	17
$B_2(10)$	(005)	727	474	—	1.7×10^{-4}	0.0142	18
$B_2(11)$	(201)+(021)/[101]	742	489	—	0.0012	0.0117	17
$B_2(12)$	[200]	759	506	—	1.2×10^{-4}	0.0025	18
E(1)	(100),(010)	427	174	160	0.1701	0.1701	8
E(2)	[000]	450	197	—	0.0024	0.0026	11
E(3)	(101),(011)	515	262	271	0.0466	0.0666	11
E(4)	[001]	559	306	316*	0.0147	0.0275	13
E(5)	(102),(012)/[001]	608	355	345*	0.0086	0.0256	15
E(6)	[100]	634	381	—	0.0035	0.0132	15
E(7)	[002]	678	425	—	0.0034	0.0207	15
E(8)	[010]	685	432	—	6.5×10^{-6}	4.26×10^{-5}	15
E(9)	(300),(030)	699	446	—	0.0015	0.0113	17
E(10)	(103),(013)/[002]	728	475	—	0.0018	0.0226	17
E(11)	[101]	752	499	—	0.0011	0.0150	17
E(12)	[200]	767	514	—	4.3×10^{-4}	0.0087	17

The lowest excited state has B_2 symmetry (it transforms as the function z), and lies 108 meV above the ground state. Its wavefunction (figure 5) shows that it corresponds closely to a first excited oscillator state for vibration along the z (tetragonal) axis. For states such as this, which can be clearly identified as oscillator states, we indicate the oscillator state in table 1 by the notation (lmn), where l, m and n are the quantum numbers for vibration in the x, y and z directions (see figure 1). Thus, the lowest excited state is identified as (001). It has often been observed experimentally, and its measured excitation energy is 115 meV (Ikeda and Watanabe 1987), so that our value is slightly low.

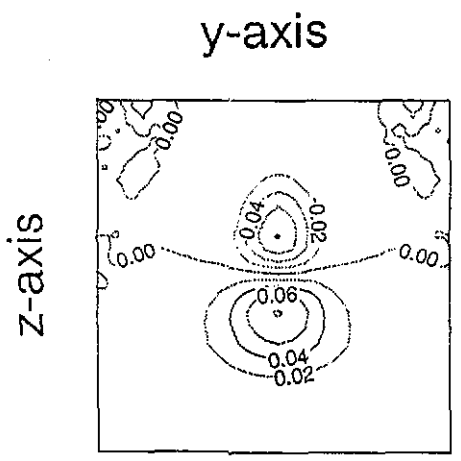

Figure 5. The wavefunction of the first excited state $B_2(1)$ shown as a contour plot on the y–z plane. The edges of the plot are equal to $\frac{1}{2}a_0$ in each direction.

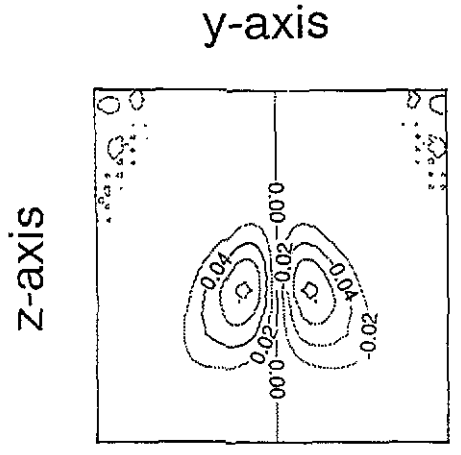

Figure 6. The wavefunction of the second excited state E(1) shown as a contour plot on the y–z plane. The edges of the plot are equal to $\frac{1}{2}a_0$ in each direction.

The next excited level, which lies 174 meV above the ground state, is doubly degenerate and has E symmetry. It is clearly identified as the pair of oscillator states

(100) and (010) by the contour plot shown in figure 6. The calculated excitation energy is slightly higher than the experimental value of 160 meV (Ikeda and Watanabe 1987).

The oscillator interpretation leads one to expect the state (002) having A_1 symmetry at an energy of $\sim$ 200 meV. In fact, the situation is more complicated. We find two closely spaced states of this symmetry, whose wavefunctions are displayed in figure 7. Both these states have the form expected for (002) near the central site, but in addition they have substantial weight on neighbouring tetrahedral sites. They can be regarded as linear superpositions of (002) on the central site and oscillator ground states on neighbouring sites. To express this more clearly, let us denote by $\psi_{002}^{(0)}$ the oscillator state (002) on the central tetrahedral site, and by $\psi_0^{(i)}$ an oscillator ground state on neighbouring tetrahedral site i ($i = 1$–4). Since we are dealing with A_1 symmetry, the $\psi_0^{(i)}$ must appear in the combination $\Psi_0 = \frac{1}{2}(\psi_0^{(1)} + \psi_0^{(2)} + \psi_0^{(3)} + \psi_0^{(4)})$. The two states shown in figure 7 are then the two linear combinations:

$$\begin{aligned} \psi_+ &= \cos\theta\ \psi_{002}^{(0)} + \sin\theta\ \Psi_0 \\ \psi_- &= -\sin\theta\ \psi_{002}^{(0)} + \cos\theta\ \Psi_0 \end{aligned} \tag{10}$$

where θ is some mixing angle. As expected, the lower of the two states ψ_+ displays constructive interference between $\psi_{002}^{(0)}$ and Ψ_0 in the region between the sites, while ψ_- displays destructive interference, with a nodal surface in this region. The strong mixing arises from the near coincidence of the energies of (002) and of the ground state on neighbouring sites. Such a coincidence must surely be very sensitive to the details of our interaction model, and it may not occur in the real system. In spite of this uncertainty, the two states together can be confidently identified with the experimentally observed transition at 220 meV (Ikeda and Watanabe 1987). As with the (001) state, our predicted excitation energy is slightly low.

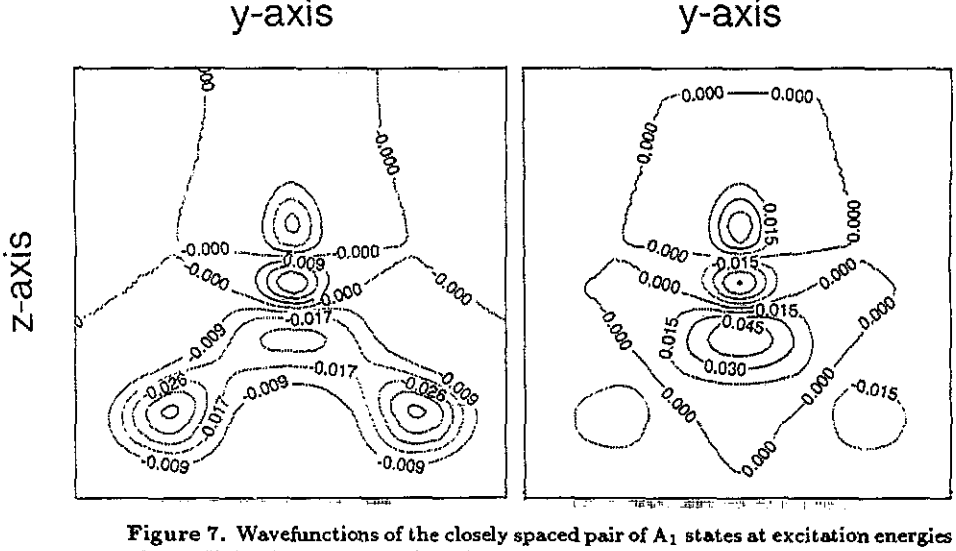

Figure 7. Wavefunctions of the closely spaced pair of A_1 states at excitation energies of 195 eV (left) and 205 eV (right), shown as contour plots on the y–z plane. The edges of the plots are equal to $\frac{3}{4}a_0$ in each direction.

Linear combinations of the five functions $\psi_{002}^{(0)}$ and $\psi_0^{(i)}$ are expected to yield five eigenstates. The three states not accounted for by ψ_+ and ψ_- must be linear combinations of the $\psi_0^{(i)}$ alone, and it is readily verified that these must consist of a state of B_2 symmetry and a degenerate pair of E symmetry. A glance at table 1 confirms the presence of these three states at energies almost identical to those of the two A_1 states. Examination of their wavefunctions (not shown here) shows that they are concentrated almost entirely on the neighbouring tetrahedral sites, and are therefore unlikely to be experimentally observable; this will be confirmed by our results for the transition intensities presented in the next section.

Detailed study of the other states listed in table 1 shows that in almost all cases they can be thought of as linear combinations of oscillator states on the central and neighbouring tetrahedral sites. This gives a way of characterizing most of the states in the table. We continue to use the notation (lmn) to denote oscillator states on the central site. For eigenfunctions which can be represented as linear combinations of oscillator states on neighbouring tetrahedral sites alone, we shall use the notation $[\lambda\mu\nu]$; any eigenfunction so labelled consists approximately of oscillator states having quantum numbers λ, μ and ν on the neighbouring sites. It should be noted here that ν is the quantum number for vibration along the tetragonal axis at the tetrahedral site in question (i.e. along the direction from that site to a neighbouring octahedral site), rather than the tetragonal axis at the central site; likewise, λ and μ refer to motion in directions perpendicular to the local tetragonal axis. For eigenfunctions which involve substantial mixing between oscillator states on both central and neighbouring sites, we use the notation $(lmn)/[\lambda\mu\nu]$. We shall not try to make more precise what counts as 'substantial' here. Finally, there are a few states which are constructed mainly from oscillator ground states on *second-neighbour* tetrahedral sites; we indicate these by {000}. We have used the above notations to characterize most of the eigenfunctions listed in table 1.

From this discussion, and from the large deviations of $w(\boldsymbol{r})$ from the oscillator form, it might be expected that the wavefunctions of all the higher states would be distributed in a complicated way over several sites. Remarkably, this turns out not to be the case. Three of the higher states in particular are strongly localized on the central site: E(3), $B_1(1)$ and $A_2(2)$, which have respectively excitation energies of 262, 386 and 485 meV. The wavefunctions of the first two of these are shown in figure 8. The oscillator character of the states is beautifully clear, and indeed the anharmonic distortions seem no stronger than for the two lowest excited states $B_2(1)$ and E(1). The same is true of the state $A_2(2)$ (not shown here). We shall see in the following section that the first of these three states has a substantial transition intensity, and it can be confidently identified with one of the inelastic peaks observed by Ikeda and Watanabe (1987). The intensities of the other two states, particularly $A_2(2)$, are much smaller, and they cannot be identified with any confidence in the experimental spectrum.

Also included in table 1 is a comparison with experimental transition energies. The assignment of experimental peaks for highly excited states is problematic, as we shall discuss in more detail in the next section.

5. Transition intensities

We have calculated the spherically averaged intensities $\langle I_i(Q)\rangle$ defined in section 2.5

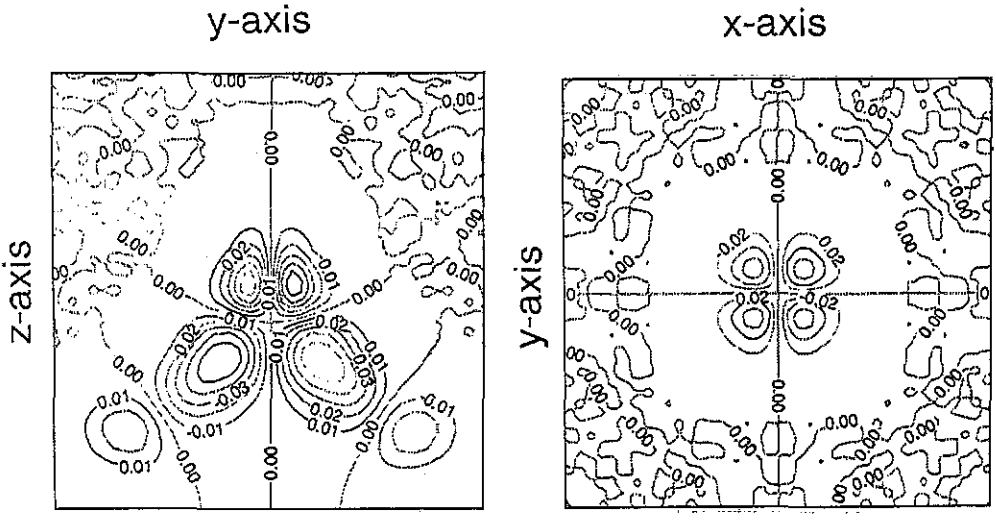

Figure 8. Wavefunctions of the highly excited states E(3) (left) and $B_1(1)$ (right) shown as contour plots on the planes y–z and x–y respectively. The edges of the plots are equal to $\frac{3}{4}a_0$ in each direction.

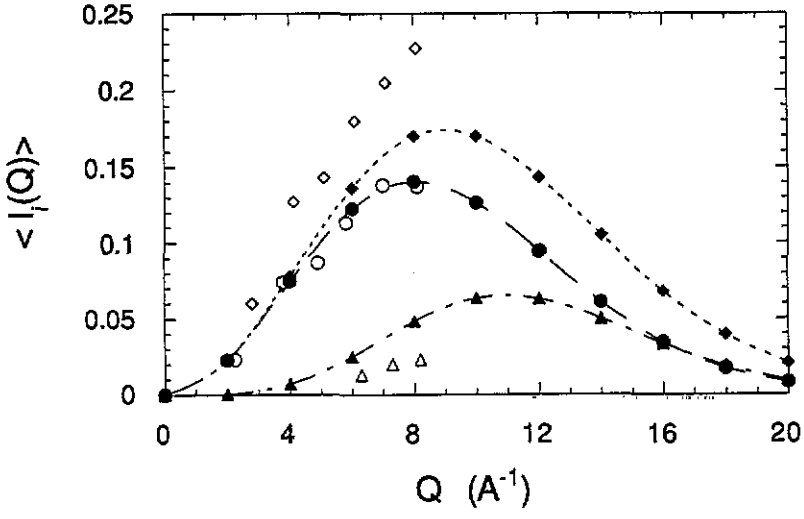

Figure 9. Comparison of calculated and experimental intensities $\langle I_i(Q)\rangle$ as a function of wavevector transfer Q for the lowest excited states $B_2(1)$ (circles), E(1) (diamonds) and $A_1(2$ and $3)$ (triangles). Calculated and experimental results are shown by filled and open symbols respectively . Curves passing through calculated values are a guide to the eye.

for all the states listed in table 1, and for wavevectors Q going from 0 to 20 Å^{-1}. We report in table 1 the intensity of each state for $Q = 8$ Å^{-1}. The reason for choosing this Q is that it is the highest wavevector transfer achieved in the experiments of Ikeda *et al* (1990); the intensities of the experimentally observed transitions increase monotonically up to this value of Q. We also show in the table the maximum value $\langle I_i(Q_{max})\rangle$ of each intensity, together with the wavevector Q_{max} at which this maxi-

mum value is attained. It should be noted that for E states the intensities given in the table include the factor of 2 for the double degeneracy.

For the three lowest excited states, we can compare our results directly with the experimental values given in figure 6 of the paper by Ikeda *et al* (1990). There is a slight ambiguity here, since their figure presents the intensities in 'arbitrary units'. We have removed this ambiguity by making use of the comparison with analytical formulae presented in the same figure. Our calculations are compared with the resulting experimental values in figure 9. We stress that these experimental values have been brought to the form needed for making a direct comparison with our $\langle I_i(\boldsymbol{Q})\rangle$.

Our calculated intensity for the lowest excited state (001) is in very close agreement with the experimental values, which suggests that our wavefunction for this state is essentially correct. However, the agreement for the next state E(1), i.e. the degenerate pair of oscillator states (100) and (010), is much poorer: our predicted intensity is low compared with the experimental values by about 25%. This seems to suggest that our wavefunction for this state is not fully realistic, even though the calculated energy agrees quite well with experiment. Our predicted intensity for the third excited state (002) is in even poorer agreement with experiment, being too high by about a factor of two. These disagreements suggest that our interaction model must be in error in significant respects.

Although our calculated intensities for the higher excited states cannot yet be compared with experiment, they are useful, because they confirm the experimental observability of some states, and allow us to rule out many others as unobservable. This simplifies the task of identifying the experimental peaks with our calculated states. We note in particular the relatively high intensity of the transitions to the degenerate pair (101), (011), which allows us to identify them with the prominent experimental peak at 271 meV. In attempting to identify the other peaks, we have arbitrarily assumed that transitions whose intensities are less than 0.005 at $Q = 8$ Å^{-1} would not have been observed by Ikeda and Watanabe. On this basis, we have made the experimental assignments given in table 1. It must be stressed that some of the assignments are tentative, and must remain so pending more detailed experiments.

There is a puzzling feature that we have not been able to resolve. The experiments show pronounced peaks at 400 and 450 meV. Before performing the present analysis, we were convinced that the peak at 450 meV would be identified with the well-defined oscillator state (111). However, our calculations seem to show that its transition intensity would be too small to have been observed by Ikeda and Watanabe (though it might become observable at higher values of Q). Equally puzzling is the fact that our calculations do not yield any plausible candidate for the peak at 400 meV.

6. Discussion

The aims of this work have been (i) to demonstrate an effective method for making detailed calculations on the quantum states of hydrogen in transition metals; (ii) to use this method to investigate the nature of the ground state and a wide range of excited states of H in Nb; (iii) to suggest how such calculations can be used to test models for the metal–hydrogen interaction; (iv) to provide tools for interpreting the results of neutron inelastic scattering experiments.

The calculation methods we have developed build on the pioneering work of Fukai and Sugimoto. However, our more efficient calculation methods and our full use of

symmetry have allowed us to go very much further than them. We have been able to test in some detail the numerical approximations, and, more importantly, to make calculations on a wide range of highly excited states, which are beginning to be studied experimentally.

In discussing the characteristics of the states revealed by our calculations, one has to be aware that everything is based on an assumed interaction model. However, it is a model which has already been shown to produce reasonable results for the temperature-dependent diffusion coefficient (Gillan 1991) and for the spatial probability distribution of hydrogen and its isotopes in niobium (Christodoulos and Gillan 1991). As we have seen, it reproduces with reasonable accuracy the measured low-lying excitation energies, and also the experimental value for the displacement of the relaxed nearest-neighbour metal atoms. It is therefore likely that it gives at least a qualitatively correct account of the higher states. We agree with previous authors in finding that the two lowest excited states closely resemble the harmonic oscillator first excited states for vibration along and perpendicular to the tetragonal direction. For higher excitation energies, the potential is so different from an oscillator potential that many of the higher states cannot be thought of simply as oscillator states. We have shown that a more correct way of viewing these states is as linear combinations of oscillator states on the central and neighbouring tetrahedral sites. Many of the excited states, beginning with the oscillator state (002), have some of their weight concentrated on neighbouring sites. It need hardly be said that states involving this kind of mixing on different sites could never emerge from the kind of low-order perturbation treatment used in some recent analyses, and we believe that the perturbation approach is simply incorrect for some of the higher excited states. In spite of this, our calculations show the existence of well-characterized states having clearly defined oscillator features up to excitation energies of nearly 0.5 eV. This encourages us to think that a clear interpretation will be found for many of the experimentally observed transitions. We cannot yet provide such an interpretation with any confidence simply by comparing our predicted excitation energies with the observed transition energies, because our interaction model is not sufficiently reliable, and because the assignment of the higher experimental transitions is uncertain.

The comparisons with experiment that we have been able to make have given useful tests of the interaction model, and indeed have shown that the model needs improving. The excitation energies of the states $B_2(1)$, $A_1(2)$ and $A_1(3)$ are low compared with experiment by 6% and 10% respectively, while that of the degenerate pair E(1) is too high by 8%. This suggests that the tetragonal anisotropy produced by our model is too great in this energy range. Strong confirmation for this comes from the comparison of our calculated wavevector-dependent intensities with experiment. For an isotropic oscillator, the intensity of the degenerate pair E(1) would be twice that of $B_2(1)$, in rough accord with experiment, whereas our calculated wavefunctions yield a much lower ratio. The development of a more satisfactory interaction model will be an important task for the future. We note here our belief that important support for the development of improved potentials in this and other systems will come from *ab initio* electronic-structure calculations. Recent work based on the local density approximation has shown the feasibility of making *ab initio* calculations of the total energy for metal–hydrogen systems with the required accuracy (De Vita and Gillan 1991; Soler, private communication).

We hope that the theoretical apparatus we have developed for calculating transition intensities will be helpful in unravelling the experimental assignments. We have

shown that there are large numbers of excited states in the range covered by the experiments, but that many of these have unobservably small intensities. We expect that the wavevector dependences of the intensities which we are now able to calculate will provide signatures that will allow the more certain assignment of experimental peaks. Experiments on H in Nb now in progress (Bennington, private communication) aimed at observing inelastic intensities up to high wavevector transfers are expected to be very helpful in this respect.

The methods described here are currently being extended to study hydrogen and its isotopes (including the positive muon) in other transition metals, and we also plan to apply them to the calculation of tunnelling frequencies.

Acknowledgment

We gratefully acknowledge financial support from the Science and Engineering Research Council.

References

Atkins P W 1983 *Molecular Quantum Mechanics* (Oxford: Oxford University Press) ch 7
Christodoulos F and Gillan M J 1991 *Phil. Mag.* B **63** 641
De Vita A and Gillan M J 1991 *J. Phys.: Condens. Matter* **3** 6225
Eckert J, Goldstone J A, Tonks D and Richter D 1983 *Phys. Rev.* B **27** 1980
Finnis M W and Sinclair J E 1984 *Phil. Mag.* A **50** 45
Fukai Y and Sugimoto H 1985 *Adv. Phys.* **34** 263
Gillan M J 1986 *J. Phys. C: Solid State Phys.* **19** 6169
—— 1987 *Phys. Rev. Lett.* **58** 563
—— 1988 *Phil. Mag.* A **58** 257
—— 1990 *Computer Modelling of Fluids, Polymers and Solids* ed C R A Catlow, S C Parker and M P Allen (Dordrecht: Kluwer) p 155
—— 1991 *J. Less Comm. Met.* **172–174** 529
Ikeda S, Furusaka M, Fukunaga T and Taylor A D 1990 *J. Phys.: Condens. Matter* **2** 4675
Ikeda S and Watanabe N 1987 *J. Phys. Soc. Japan* **56** 565
Kimball G E and Shortley G H 1934 *Phys. Rev.* **45** 815
Klamt A and Teichler H 1986 *Phys. Status Solidi* b **134** 103
Kondo J 1985 *Physica* B **125** 279
Peisl H 1982 *Point Defects and Defect Interactions in Metals* (Amsterdam: North-Holland) p 41
Puska M J and Nieminen R M 1984 *Phys. Rev.* B **29** 5382
Springer T 1978 *Hydrogen in Metals I (Springer Topics in Applied Physics 28)* ed G Alefeld and J Völkl (New York: Springer) p 75
Stoneham A M 1975 *Theory of Defects in Solids* (Oxford: Clarendon)
Sugimoto H and Fukai Y 1980 *Phys. Rev.* B **22** 670
—— 1981 *J. Phys. Soc. Japan* **50** 3709
—— 1982 *J. Phys. Soc. Japan* **51** 2554